Journal of South American Earth Sciences 104 (2020) 102850

Contents lists available at ScienceDirect

Journal of South American Earth Sciences

journal homepage: www.elsevier.com/locate/jsames

Ongoing automated ground deformation monitoring of Domuyo - Laguna del Maule area (Argentina) using Sentinel-1 MSBAS time series: Methodology description and first observations for the period 2015–2020

Dominique Derauw [a,b,c,*], d'Oreye Nicolas [b,d], Maxime Jaspard [b], Alberto Caselli [a], Sergey Samsonov [e]

[a] Laboratorio de Estudio y Seguimiento de Volcanes Activos (LESVA), IIPG - Universidad Nacional de Rio Negro – CONICET, 1242 Av. General Roca, 8332, General Roca, Argentina
[b] European Centre of Geodynamics and Seismology (ECGS), 19 rue Josy Welter, L-7256 Walferdange, Luxembourg
[c] Centre Spatial de Liège (CSL), Avenue du Pré Aily, B-4031 Angleur, Belgium
[d] National Museum of Natural History (NMNH), 19 rue Josy Welter, L-7256 Walferdange, Luxembourg
[e] Canada Centre for Mapping and Earth Observation, Natural Resources Canada (NRCAN), 560 Rochester Street, Ottawa, ON K1A 0E4, Canada

ARTICLE INFO

Keywords:
InSAR time series
Domuyo
Laguna del maule
MSBAS
Displacement monitoring

ABSTRACT

Synthetic Aperture Radar (SAR) Differential Interferometry (DInSAR) and its extensions to manage time series are nowadays well-known and mastered techniques to perform among others land-motion monitoring.

We present here a fully automated monitoring service based on DInSAR and Multidimensional Small Baseline Subset (MSBAS) methods. The automated processing chain named **"InSAR automated Mass processing Toolbox for multidimensional Time series" (MasTer)** is demonstrated with the peculiar case of the Laguna del Maule and Domuyo volcanoes, which are known to undergo significant inflation up to several cm or tens of cm per year.

The here-described monitoring service is made of three components: an InSAR command line processor, the MSBAS processor and a number of shell scripts automatizing all tasks, from data downloading to updated displacement maps and time series. Thanks to the European Commission Copernicus Service, data are freely available every 12 or 6 days along each orbit, depending on ESA acquisition plan. Linear deformation rate maps and time series of vertical and East-West ground deformation computed by the MasTer tool are updated every 1–6 days on a web page, according to the S1 data availability. Interested user can request additional time series at coherent pixels that wouldn't be displayed on the web page and receive them by e-mail within a minute.

Processing chain and preliminary observations at Domuyo and Laguna del Maule test site are presented and commented. The nearly 6 years long 2D time series of ground deformation allow highlighting recent changes in the well-known deformation at both volcanoes: Domuyo inflation stabilizes since beginning of 2019 while deformation at Laguna del Maule seems to gently accelerate since mid 2018. New deformation features are also identified, such as a 2 km wide 3 cm/yr circular subsidence at Laguna del Maule as well as a 2 cm/yr downward and 1 cm/yr eastward movement located to the East of Laguna Fea.

1. Introduction

Synthetic Aperture Radar (SAR) Interferometry (InSAR) is a well-established method to compute digital elevation models or measure ground deformation [Massonnet and Feigl, 1998]. Differential SAR Interferometry (DInSAR) takes advantage of phase measurement difference between two SAR images acquired at two different dates to infer line of sight component (LOS) of displacements occurring in that time lap [Massonnet et al., 1993].

Earth observation satellites that offer recurrent SAR observations are following sub-polar helio-synchronous orbits generally imaging the scene sending their illuminating radar beam on their right with respect to the satellite velocity vector. This defines ascending or descending acquisition modes of the satellite while going from South to North Pole

* Corresponding author. European Centre of Geodynamics and Seismology (ECGS), 19 rue Josy Welter, L-7256 Walferdange, Luxembourg.
E-mail address: dderauw@unrn.edu.ar (D. Derauw).

https://doi.org/10.1016/j.jsames.2020.102850
Received 20 May 2020; Received in revised form 5 August 2020; Accepted 26 August 2020
Available online 3 September 2020

or conversely.

As a consequence, the DInSAR displacement estimated along an ascending orbit is computed in a sub-East-West line of sight, while along descending passes it is provided in a sub-West-East line of sight.

In principle DInSAR is able to give displacement estimates with a millimeter precision. However, some limitations may hinder the technique, mainly in natural environment. Spatial and temporal signal de-correlation are the principal causes that prevent performing sound interferometric measurements and in turns, correct local displacements estimates.

Temporal de-correlation corresponds to changes over time in the backscattering behaviour of the ground targets. This includes single scatterers physical characteristics changes but also scatterers distribution changes inside the imaged pixel. Temporal de-correlation can only be tackled considering SAR acquisition time difference short enough to minimize temporal changes of observed scenes or time base allowing to recover for structural pixel changes, like seasonal cycles.

Spatial (or geometrical) de-correlation is proportional to the perpendicular baseline, i.e. the perpendicular distance between the sensor position at respective acquisition time. Increasing perpendicular baseline changes the angle under which a given element of the scene is observed. As a consequence, although the physical characteristics of the scatterers do not change, their relative responses in terms of optical path difference differ. The largest perpendicular baseline below which correlation is preserved depends on the SAR wavelength, the distance from the satellite to the ground (i.e. the range) and the local incidence angle. Typically, in C band, for uniform scatterers distribution on flat areas, the perpendicular baseline should remain below some tens to some hundreds of meters [Zebker and Villasenor 1992]. Note that techniques named Persitent Scatterers (PS) Interferometry [Ferretti et al., 2001] consider point scatterers as the measurements probes instead of natural surfaces made of uniform scatterers distributions, which allows considering larger perpendicular baselines. However, PS's are barely present in natural environment, which is why PSInSAR is mostly used in urban context and not considered here.

Impact of both de-correlation sources is assessed through coherence estimation. Physically speaking, coherence is a measurement of the ability of two wave fronts to stay spatially and/or temporally in phase. This is a mandatory condition to get an interpretable interferometric pattern and in turn, obtain a valid local displacement estimate. Coherence is thus the very first quality indicator of any interferometric measurement, whatever the domain of Physics we are speaking about. In SAR interferometry, selecting appropriate combination of short spatial baselines and short revisiting times optimizes the chances to get the highest possible coherence. However, in some cases, longer temporal baselines may be useful. On the one hand, considering baseline of around one seasonal cycle may allow recovering highly similar surface conditions leading to partial coherence recovery. On the other hand, short temporal baseline may limit the signal to noise ratio, that is the measurement precision with respect to displacement amplitude, e.g. when tracking long term, slow and continuous displacement.

Selecting every convenient interferometric pair satisfying optimum spatial and temporal baselines to derive a time series of displacement estimate on a given time interval is the basis of the Small Baseline Subset technique (SBAS) [Berardino et al., 2002]. Provided all the selected time intervals cover the total large timespan and possibly intersects between themselves, DInSAR time lap measurements allow, through problem inversion, getting the full displacement time series for areas keeping a sufficient coherence level in all considered interferometric pairs. SBAS method is commonly used nowadays and proved to be efficient and reliable in several contexts [e.g. Galve et al., 2017; Doin et al., 2011], including the area under concern in this paper [Lundgren et al., 2020; Novoa et al., 2019; Zhan et al., 2019].

Because of the geometrical constrains required to preserve the coherence, DInSAR can only be performed with SAR images acquired in the same mode (same sensor family and same viewing geometry). Therefore SBAS time series provide the evolution in time of the component of the displacement along this line of sight. If using a single acquisition mode, one has to make hypothesis on the observed displacements under concern to project this line of sight estimate along the known or supposed displacement axis in 3D. This displacement axis ambiguity can however be solved, or partly solved, if having enough different observing modes giving each a time series displacement along different lines of sight.

A consistent solution was developed while directly considering the inversion problem in 2 or 3 dimensions, in geographic coordinates. This approach is called the Multidimensional Small Baseline Subset (MSBAS) processing [Samsonov and d'Oreye, 2012, 2017; Samsonov et al., 2017, 2020]. It is an extension of the SBAS method that allows inverting simultaneously several interferometric SAR time series acquired along different acquisition modes, including different sensors, SAR wavelengths, incidence angles, polarization etc., to solve for horizontal and vertical component of the ground displacement. However, because SAR satellites nowadays circling the globe acquire data in a side-view geometry along subpolar orbits, InSAR measurements are nearly insensitive to displacements occurring in the North-South direction. This usually restrict the inversion to the vertical and East-West components. MSBAS can retrieve the full 3D decomposition only in some specific cases, such as slow-moving landslides or glacier flows, when one can reduce the degree of freedom by assuming that the displacements occur parallel to the surface [Samsonov et al., 2020]. However, because this is restricted to rare applications, MasTer tool described here only deals with the inversion in 2D, that is the vertical and East-West directions. This approximation was shown to be valid as long as the displacement in the North-South component is not significantly larger than in the other directions [Samsonov and d'Oreye, 2012; Nobile et al., 2018].

To feed the MSBAS processor, one need to compute differential InSAR phase maps, projected in geographic coordinates. For each mode, one has to define a maximum perpendicular baseline and a maximum time lap to optimize coherence conditions. This will lead to a given number of interferometric SAR pairs to be processed up to the generation of geo-projected differential phase maps.

During years, the main bottleneck for applying SAR time series analysis for displacement monitoring was data provision due to restrictive data policies, data cost and/or low observation frequency. The European Copernicus Sentinel1 constellation drastically changes the situation in all these aspects: free data access (in both acceptations of the term: free access and free of charge) at systematic and recurrent acquisition pace. Depending on the area, every 24, 12 or even 6 days, a SAR image is acquired allowing to build long and systematic time series. Additionally, Sentinel1 constellation is flying within a small orbital tube granting baselines generally below 120m, whatever the considered image pair. Therefore, combining ascending and descending Sentinel1 time series in MSBAS processing allows solving for vertical and horizontal components of the observed displacements.

While opening a new era, Sentinel1 is also opening new challenges in terms of processing load and data storage management. Automation became a prerequisite to efficient InSAR time series and MSBAS processing. Additionally, optimization aspects in both terms of computation load and data storage are mandatory if willing to maintain laboratory-scale facility.

It is in this respect that we developed an automated InSAR Mass processing Toolbox for Multidimensional time series (MasTer) [d'Oreye et al., 2019; d'Oreye and Derauw, 2020].

Other automatic InSAR processing tools are available for producing interferograms and deformation maps (among others) such and MOUNTS [Valade et al., 2019] or LiCSAR [Lazecky et al., 2020]. Some systems also produce semi-automatic or automatic time series of ground deformation either using PSI or SBAS techniques, or both, such as LiCSBAS [Morishita et al., 2020], InSAR Viewer [Yunjun et al., 2019], SNAP-StamMPS [Delgado Blasco et al., 2019], P-SBAS [De Luca et al., 2018], or SqueesSAR [Raspini et al., 2018]. However, to our knowledge,

no other tool allows a fully automatic production of unsupervised 2D ground deformation time series (from data download as soon as a new image is available, up to updated times series made available on a web page), without limitation in ground resolution (other than the one from the satellite data) and able to combine any type of SAR data.

MasTer is maintained and managed at the European Center for Geodynamics and Seismology (ECGS), where it is routinely used among others to automatically monitor ground deformation in the Virunga Volcano Province (Democratic Republic of Congo) and in Luxembourg and the Greater Region. The Royal Museum of Central Africa (Belgium) and the Geological Survey of Austria also use MasTer to study landslides respectively in the South Kivu province (Democratic Republic of Congo) and in Austria [Samsonov et al., 2020; Nobile et al., 2018; Dille et al., 2020; Hormes et al., 2020]. For sure, MasTer is also used at Laboratorio de Estudio y Seguimiento de Volcanes Activos (LESVA), Rio Negro, Argentina.

The present paper aims at providing an overview of the tool and presenting its specificities. We describe some optimization aspects in the InSAR processing chain allowing its use on classical computers or workstations. Finally, we present results routinely and automatically computed on the Domuyo and Laguna del Maule area. This processing is performed and updated daily without human interaction, from data download to final deformation maps and ground deformation time series displayed on a dedicated webpage.

2. MasTer tool description and implementation

MasTer tool is a set of mostly shell scripts aiming at processing automatically a large number of interferometric pairs and feeding and running the MSBAS processor [Samsonov and d'Oreye, 2012, 2017; Samsonov et al., 2017, 2020] in order to obtain the desired deformation maps and time series in vertical and horizontal components. Geocoded amplitude, coherence, interferometric phase and deformation maps are computed using the MasTer Engine, a command line InSAR processor derived from the Centre Spatial de Liege (CSL) InSAR Suite (CIS) [Derauw, 1999; Derauw et al., 2019]. CIS is able to process any type of SAR data (ERS1 & 2, EnviSAT, ALOS, ALOS2, RADARSAT 1& 2, COSMO-SkyMed, TerraSAR-X, TanDEM-X (incl. bistatic and pursuit mode), Sentinel1 A & B, Kompsat5, PAZ, SAOCOM…). The CSL InSAR Suite was modified and optimized to fit the needs of the MasTer tool, which benefitted from some of its unique specificities. The tool is illustrated here with Sentinel 1 data but can be performed with, or in combination with any other SAR mission, which could ultimately lead to denser time series and higher updating rate of the results displayed on the web page.

2.1. The MasTer tool shell scripts

MasTer performs all its tasks thanks to a series of scripts launched by few command lines which are easily integrated in cron jobs to become a fully automated tool. The whole processing chain makes use of single files containing all the parameters required for the mass processing of each satellite mode.

The processing chain is designed to split the work in several tasks, some of which can be run in parallel. These tasks are optimized e.g. by sharing intermediate results that are common between some steps. It is self-evaluating and able to automatically tune some parameters and recompute some steps that would be unsatisfactory. Computation of time series is incremental, that is, when a new image is available, MasTer downloads it automatically, then computes the new interferometric pairs formed using this new image along with all the images already acquired that satisfy the pre-defined spatial and temporal baselines criteria. The new differential deformation maps are then added to the existing database to be inverted by MSBAS. To compute the vertical and horizontal (EW) linear rates and the cumulative deformation maps and time series, the MSBAS inversion itself only takes few tens of minutes to hours depending on the size of the area and the number of pairs. The processing architecture is also designed in order to minimize the loss of data in case of hardware failure by storing the data and the intermediate and final results in a directories structure that is easily shared between several dedicated hard disks or servers.

We describe below a typical processing chain such as the one used for the monitoring of the Domuyo/Laguna del Maule region using Sentinel 1 (S1) data presented here after.

1. A first script sub daily checks if new S1 data or updated orbits are available on the data provider's server. Newly available data are downloaded and read, that is transformed in the InSAR Suite internal format. At this stage, all and only the relevant swaths and bursts are selected. If the provided area of interest encompasses several S1 frames or is at the intersection of two consecutive S1 frames, image stitching is automatically performed to consider requested bursts only. If precise orbits are made available (usually within 3 weeks after image acquisition), images are not downloaded again. Instead, only orbit information is updated, and each step of the processing chain affected by that update, for every interferometric pair involving the concerned date, is recomputed.
2. After each new or updated image, MasTer selects the pairs that fit the requested spatial and temporal baselines, then update the corresponding baseline plots. The super-master is selected at this stage during the first run. For routine monitoring, it is not advised to change super master as it would require to recompute the entire database of interferometric pairs in that new geometry.
3. For all but Sentinel 1 sensor, each new image is then coregistered with the super master and the digital elevation model and optional mask are projected in the master slant range geometry. For S1 images, digital elevation model and optional mask are projected in each image slant range geometry. For non S1 data, optional crop can be performed here as well.
4. Each and only new pairs satisfying the baselines criteria selection performed at step 2 is then processed up to the geocoding of each interferometric product: amplitude, coherence, interferometric phase, differential interferometric phase, unwrapped phase, deramped unwrapped phase (optional), interpolated unwrapped phase to fill up empty pixels surrounded by unwrapped values (optional), deformation map, incidence angle map…. When processing a large amount of data it is possible to split the number of InSAR processes into a number of parallel sessions chosen by the user. These sessions can be run on separate hard disks in order to minimize the performance loss due to large amount of simultaneous read and write operations on a given hard drive.
5. All InSAR products are geocoded on a grid defined in the parameter file in order to be similar for all the satellites and/or geometries. This is indeed a requirement for the MSBAS step. All the geocoded products are provided in classical ESRI-ENVI© format, which can be directly read by classical Geographic Information System (GIS) software.
6. Next, the deformation maps are fed to MSBAS in the desired format, and required description files are prepared. Note that at this step, further selection among the interferometric pairs can be performed. In particular, one can restrict the MSBAS processing to only the pairs that satisfy the baselines criteria but also that satisfy a mean coherence threshold computed over a dedicated region defined by a kmz file. This for instance may be of interest for monitoring regions that are affected by strong seasonal variations causing decorrelation from the summer to winter transition while preserving coherence from summer to summer (e.g. free from snow cover). Test can be further performed here to identify interferograms affected by unwrapping error. This is done by checking phase closure consistency between triangles of pairs [Benoit et al., 2020, Morishita et al., 2020]: for each triplet of interferograms spanning 3 dates (says date1-date2, date2-date3 and date1-date3), the mean unwrapped phase Φ_{ij} (where i and

j are the index of the date) is computed over an area defined by a user-provided kml file. If $|\Phi_{13} - (\Phi_{12} + \Phi_{23})|$ is larger than a chosen threshold, the triplet of interferograms are flagged as affected by possible unwrapping errors. Comparing all the flagged triplets allows identifying the faulty interferograms, which must be manually checked and/or removed from the database.

7. MSBAS inversion is then performed taking into account all the former and new deformation maps in each mode. Linear deformation rates can be computed with respect to a selected pixel (or set of pixels) supposed to be stable or for which the behavior is well known (e.g. monitored by another geodetic method such as GNSS). In the present case, deformation maps are not referred to a specific region but the average is set to zero instead. MSBAS linear deformation rates and cumulative deformation maps in vertical, horizontal and/or LOS components as well as error maps are provided in GIS format. Quick look raster images, or kmz maps to be displayed in Google Earth are computed. If provided with a list of pixels coordinates, it will compute time series graphs for as much pixels of interest as desired. Graphs of double difference time series can also be performed.
8. Finally, linear deformation rate maps in vertical, horizontal and/or LOS directions as well as graphs of time series displacements at selected pixels are synchronized on a web server for displaying in an optionally password protected web page.

MasTer tool offers the possibility to extract and plot the time series of ground displacement at any pixel where coherence is preserved in each interferometric pair used for the MSBAS inversion. It also offers the possibility to compute the double difference between time series of two pixels, which allows reducing noise from common sources such as atmosphere and eliminating the influence of the reference region taken for the time series. Optional linear fit can be added to the plot. As much pixels as requested can be displayed; selection is provided to MasTer through a simple list of coordinates (in lines and columns index from the deformation maps, in GIS logic, that is the origin is in the upper left corner of the map).

Several additional tools exist for testing and fine-tuning the processing, for selecting the most appropriate MSBAS inversion parameters, or for cleaning or reprocessing only some steps after a possible crash. If an image presents some problem, it can be quarantined from the automated processing chain. Specific scripts exist to create masks based on mean coherence and/or water bodies. Other scripts allow generating sequence of amplitude gif animation to monitor the ground cover changes or the geomorphologic changes over time (see e.g. https://sentinels.copernicus.eu/web/sentinel/news/-/article/sentinel-data-support-study-of-volcanoes-and-landslides-in-africa).

2.2. The MasTer Engine InSAR processor

For consistency with the here-described automated InSAR Mass processing Toolbox for Multidimensional time series, we call the MasTer Engine, the command line InSAR processor and some preprocessing tools allowing to perform per mode image pairs selection based on input criterion of limit baseline and limit time base. The command line InSAR processor is derived from the Centre Spatial de Liege (CSL) InSAR Suite (CIS) developed internally mainly on public Belgian Science Policy (BelSPo) funding since the early nineteen's. CIS constitutes also the core of the SAOCOM InSAR Suite (SIS) internally used at CONAE.

The MasTer Engine, now maintained at LESVA, stays in continuous developments to catch up with new sensors and add new capabilities. It is a very lightweight processor coded in C that has interesting features such as:

- the ability to perform a complete InSAR processing in the geometry of a super master image. From its early conception, CIS was conceived to consider a given image as reference with respect to which a master-slave interferometric pair is co-registered [Derauw and Moxhet 1996]. All subsequent InSAR processing steps are then made in the super master image geometry, taking into account the master to super master image coregistration transform wherever required,
- the ability to perform SplitBand interferometry [Bovenga et al., 2013; Libert et al., 2017] for either absolute phase unwrapping or ionospheric decomposition,
- in line with band splitting, it allows estimating spectral coherence in a single image e.g. for vessel tracking [Derauw and Barbier 2014],
- for phase unwrapping, it allows choosing between the largely used SNAPHU [Chen and Zebker, 2001] or a homemade branch cut algorithm [Goldstein et al., 1988; Derauw 1995].
- the ability to automatically select and stitch frames, swaths and bursts of interest from TOPSAR Sentinel 1 data if giving an area of interest in input,
- The ability to perform full PolInSAR processing including coherence optimization and Pauli decomposition,
- the possibility to de-ramp both the master and the slave images at the end of the specific S1 coregistration process. This allows generating S1 Single Look Complex (SLC) images that may be used as classical ones. This is particularly useful when willing to apply techniques like coherence tracking [Pattyn and Derauw, 2002],
- the ability to calibrate Sentinel 1 amplitude images,
- the ability to use for all modalities, a common mask provided in geographic coordinates,
- the ability to geoproject all interferometric product on common predefined georeferenced frame,
- the ability to run on nearly every standard computer. For instance, it successfully computed a completed InSAR processing (up to the geoprojection) of 2 swaths and 4 bursts-large images of S1 data on an old Pentium V laptop equipped with only 2 Gb of RAM.

All scripts and software composing MasTer tool are Linux and Mac compliant.

The integrated MasTer tool was tested and validated on several areas of interest. The largest test was conducted on the Virunga Volcanic Province using a combination of more than 1.300 images acquired by ERS, EnviSAT, RADARSAT, COSMO-Skymed, TSX, TDX and Sentinel1 data, in ascending and descending modes, leading to more than 6.500 interferograms and ultimately to uninterrupted 2D deformation time series spanning 2003 to 2019 [d'Oreye et al., 2019]. It was also used to study landslide prone regions in South Kivu in DRC [Nobile et al., 2018; Dille et al., 2020], or to monitor the Greater Region spanning the Grand Duchy of Luxembourg and part of Belgium, France and Germany in the continuity of the work performed by Samsonov et al. [2013]. In all cases, excellent results were generated, offering a totally homemade and mastered processing tool for displacements monitoring, able to work without human interaction.

3. Automated and human interaction-free MSBAS monitoring of domuyo volcano and laguna del maule

3.1. Test site description

Domuyo (Neuquén province, Argentina) and Laguna del Maule volcanic complexes (Talca province, Chile) are located in the Southern Andes. This segment of the Andean orogen, which extend between 33° and 46°S, is characterized by a normal subduction of the Nazca oceanic slab beneath the South American plate with a dip angle of 25°–30°, and the development of an active volcanic arc, i.e. the Southern Volcanic Zone (SVZ) [Tassara and Yañez, 2003].

Laguna del Maule Volcanic Complex (LMVC) is one of the most hazardous active volcanic systems on Southern Andean volcanic zone [Singer et al., 2014] as suggested by the combination of an impressively large volume of Holocene silicic volcanism (36 coulees and domes from 24 separated vents surrounding a Maule lake) [Hildreth et al., 2010;

Andersen et al., 2017] and large rate of surface uplift (up to 30 cm/yr) detected since 2008 by satellite geodetic measurements [Fournier et al., 2010; Feigl et al., 2014; Singer et al., 2014; Le Mével et al., 2015, 2016].

Possible connection between the ongoing surface uplift and the activation of crustal faults is suggested by Cardona et al., [2018] who present the first detailed characterization of the seismic activity taking place at LMVC and integrate it with structural data acquired in the field. The study highlights repetitive volcano tectonic (VT) seismic swarms occurring between 2011 and 2014 at a location that roughly coincides with the intersection of two main topographic lineaments, the Troncoso and Laguna Fea Faults, of a NE-SW and WNW-ESE directions respectively. The location of the seismic swarms also coincides with the SW corner of a sill that was identified as the best fitting source of ongoing uplift by several studies inverting InSAR and GNSS measurements [Fournier et al., 2010; Feigl et al., 2014; Le Mével et al., 2015, 2016], suggesting that both faults seem to be likely activated by the inflation of the proposed sill. This hypothesis stresses the importance of monitoring the deformation in the Laguna del Maule region because the Laguna Fea Fault also borders an elevated glacial lake of the same name. If the natural dam closing the Laguna Fea lake was breached by the volcano tectonic activity, its water would be discharged to the headwaters of the Colorado River and rush through various towns, oil fields and dams, until reaching the Atlantic Ocean.

The Domuyo volcanic complex is located in the northernmost region of Cordillera del Viento (36°35′ to 36°45′S). That Cordillera is a more than 60 km long, N–S trending basement block that has been exhumed during different compressive phases of the Andean orogeny and constitutes the hinterland of the Chos Malal fold-and-thrust belt [Bracaccini, 1970; Ramos, 1977]. From upper Pliocene to lower Pleistocene times, a series of volcanic complexes developed to the east and parallel to the Main Cordillera. It includes the Domuyo volcano (4.702m asl), a Plio-Pleistocene volcanic complex considered as one of the most important igneous centers of the northern Neuquén Andes. It consists of a rhyolitic intrusive associated with early development of rhyolitic phreatomagmatic deposits and ignimbrites, and younger extrusive domes that surround the volcano on its western flank [Miranda et al., 2006]. The subsequent late Pleistocene lava flows of the Domuyo volcanic complex are referred to as “Magmatismo Dómico” (dome magmatism) by Brousse and Pesce [1982] and “Riolita Cerro Domo” (Cerro Domo rhyolite) by Llambías et al., [1978], and are exposed on the western flank of the Domuyo volcano. The western flank of the Plio-Pleistocene Domuyo volcanic complex hosts one of the world’s largest high-enthalpy geothermal fields [Chiodini et al., 2014; Tassi et al., 2016] situated more than 60 km east from the active volcanic arc. Galetto et al., [2018] propose that the dynamics of the Domuyo geothermal field is consistent with the reactivation of inherited major structures as normal faults. This reactivation could be associated to regional extensional and transtensional stresses, locally enhanced by hydrothermal effects due to the presence of a high-enthalpy geothermal fluids, likely promoting the sustainability of the geothermal field over time.

Large uplift up to 150 mm/yr in satellite line of sight was recently observed at Domuyo volcano since 2014 [Astort et al., 2019; Lundgren et al., 2020]. The hypothesis of the hydrothermal origin is challenged by a magmatic origin hypothesis. Ongoing deformation observed by InSAR could be explained by an inflating sill [Astort et al., 2019; Lundgren et al., 2020]. Magmatic reactivation from sub volcanic bodies injection would be consistent with the magmatic signature observed in gases from the hydrothermal field [Tassi et al., 2016] and the arsenic anomaly observed in the thermal and natural river waters [Morales-Simfors et al., 2020].

In that context, remote sensing, and especially MasTer, offers an efficient tool to monitor this poorly studied Domuyo volcano.

3.2. Automated measurements description

At the time of writing (July 30th, 2020), 123 Sentinel1 images acquired in ascending orbit number 18 spanning 20141030–20200718, and 182 images acquired in descending orbit number 139 spanning 20141023–20200729 are used to create 638 ascending and 1.628 descending interferograms with temporal and perpendicular baselines of maximum 450 days and 20 m respectively. The time base is chosen to encompass more than a seasonal cycle in order recover from cyclic coherence losses, mainly due to variable snow cover and to sum up large time lap DInSAR measurement within the process. The short spatial baseline (20 m) also minimizes the topographic artefacts.

Each time a new image is automatically downloaded, it is used to form new interferometric pairs with other images of the time series considering the time base and spatial baseline thresholds. New differential phase maps are then geoprojected in UTM with a pixel size of 50 × 50m and added to the existing deformation maps database. The corresponding deformation maps are then simultaneously inverted using MSBAS. However, given the seasonal snow cover in that part of the Andes, MSBAS processing is further restricted to the pairs that also satisfy a mean coherence of 0.24 computed over the Laguna del Maule region. This reduces the number of deformation maps to be inverted using MSBAS down to 926. Each deformation map is 5.361 × 4.801 pixels (i.e. more than 25 mega pixels each).

The automatic run performed on July 31, 2020 solved the system of 430 unknowns and 1352 equations in about an hour on a 72 CPU server equipped with 512 Gb of RAM.

The scripts then compute several figures (EW and UD maps and time series), then perform similar inversion separately for each mode in Line of Sight. All these results feed the web site allowing up-to-date information visualization with the shortest possible latency.

3.3. The web page

Below and introductory header, the web page displays information about the date of the last synchronization with the processing server and the date of the last images processed. Further down, the results are displayed in four different sections, accessible by scrolling down the page or by clicking on buttons.

The first panel (Fig. 1) presents color figures of linear deformation rates estimates along vertical (UD) and East-West (EW) axes (MSBAS processing) and along each LoS views (SBAS processing). Clicking on the images allows to zoom in; clicking on the “Open KMZ” blue link allows downloading the kmz color map to be displayed e.g. with Google Earth. In the present case, each SAR image acquired in Ascending and Descending orbits covers about 25.000km2 centered on the Laguna del Maule and Domuyo volcanic complexes. The common footprint, which is used for the MSBAS EW and UD decomposition, spans more than 20.000km2.

The second section of the web page shows the last ascending and descending amplitude images of the area of interest and the averages of the last 10 amplitudes images in both modes.

The third panel shows a full-size SAR amplitude image with color framed zooms indicating the location of some pairs of pre-defined points of interest. That map and the zooms can be displayed as SAR amplitude image or a Google map or a Google Earth view (Fig. 2).

Below are displayed the corresponding double difference time series of ground displacement at these pairs of points in UD & EW and in both LoS (Fig. 3). For each pair, the point used as the reference is displayed in yellow and the “moving” point is displayed in white. The double difference is computed as the moving minus the reference point (i.e. values at the white point minus the values at the yellow point). To help the reader to interpret the time series plot and understand the physical direction of the observed relative ground displacement, small explanatory sketches and location of points on the corresponding linear rate deformation maps are plotted on the side of the time series graphs, best seen

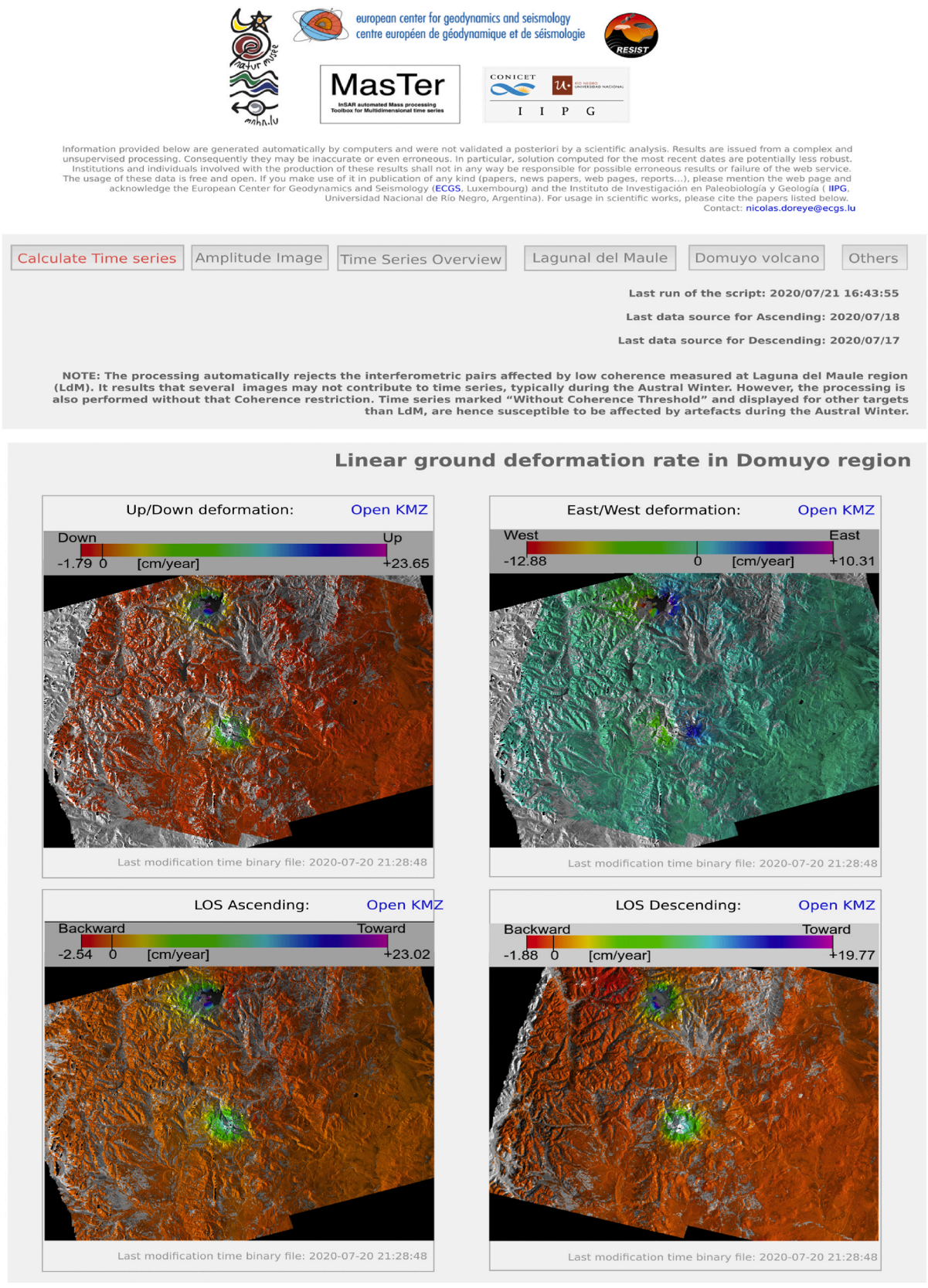

Fig. 1. First panel of web page displaying the results of the MasTer automated processing at Laguna del Maule – Domuyo region. Linear deformation rate maps computed using MSBAS processing along Up-Down (UD) and East-West (EW) directions (Above), and using SBAS processing along Ascending and Descending line of sight directions (below). Maps can be downloaded in kmz format and imported in Google Earth.

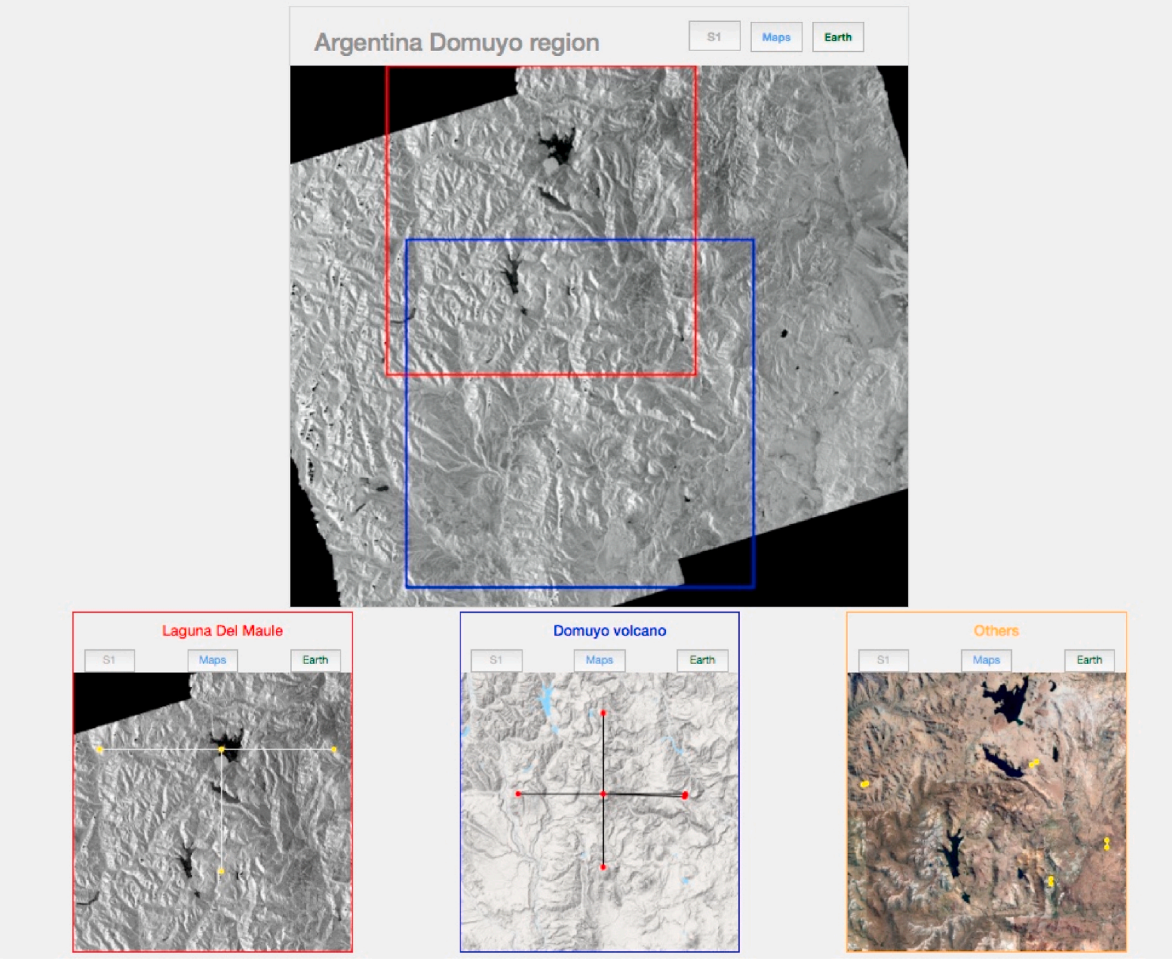

Fig. 2. Example of maps displaying the location of pairs of pre-defined points of interest at the Laguna del Maule Volcanic Complex. The user can choose to display the location on a SAR amplitude image (main map and lower left zoom), a Google map view (lower center zoom) or a Google Earth (lower right zoom).

on the full-size plot obtained by clicking on the corresponding time series (Fig. 5).

However, if the user wants to have a look at points that are not in the pre-defined list of points of interest, and hence displayed on the web page, a button allows to select new points on a map and create its own time series plots. Points selection can be done by navigating and zooming in UD, EW or LoS linear rate maps and clicking on pixels of interest. User can move the points before submitting the time series request, which will be sent to the user by e-mail within about a minute (Fig. 4).

The forth section of the web page displays the last three wrapped Ascending and Descending interferograms on Google Earth map.

The web page of the automatic MasTer processing of the Laguna del Maule – Domuyo region is openly available at http://terra2.ecgs.lu/defo-domuyo.

4. Preliminary results

As it can be easily seen from Fig. 1, both the Laguna del Maule and Domuyo volcanoes show significant uplift, with Eastward displacements of their Eastern flanks and Westward displacement of their Western flanks. Such combination of vertical and horizontal displacements corresponds to a global inflation of both volcanic complexes.

At Domuyo, the mean linear rate measured between October 2014 and July 2020 at coherent pixels close to the summit of the volcano reaches 13.5 cm/yr (Fig. 1). This is consistent with the displacement measured by Lundgren et al., [2020] between 2008 and 2019 based on RADARSAT 2, ALOS, ALOS 2 and Sentinel 1 data. These authors reported a quasi-null displacement until 2014 when it abruptly started to uplift at a roughly linear rate of 13–15 cm/yr in LoS. Thanks to the additional data now available, Fig. 3 (lower panel) and 5 (upper panel) reveal that this displacement is actually not linear. It seems to accelerate gently around early 2016. Fastest uplift occurred between 2016 and 2018 (15 cm/yr), then started to significantly decelerate since early 2019 to finally reach a plateau beginning of 2020. Future SAR observations will reveal whether this inflation is stopping or not, or if it would turn into deflation. Interestingly, considering the same dataset (with maximum 450 days and 20 m baselines) without restricting the MSBAS processing to the pairs that also satisfy a mean coherence above 0.24 computed over the summit region, underestimates the uplift by 5–10%.

At Laguna del Maule, the inflation measured as close as possible to the center of the deformation (see point marked TS in Fig. 6) is 18.4 ± 0.2 cm/yr between October 2014 and July 2018. After the 2018 Austral Winter, that inflation rate seems to have increased up to 27.0 ± 0.2 cm/yr (Fig. 5, lower panel). These values are consistent with the 15–28 cm/yr displacement rates reported by several authors for different periods spanning 2007–2017 and measured by GNSS and InSAR [Fournier et al., 2010; Feigl et al., 2015; Le Mével et al., 2015; Le Mével et al., 2016; Zhan et al., 2019, Novoa et al., 2019]. In particular, recent analysis of data recorded at a GNSS station located about 1 km west of our measurement point (station MAU2; see Fig. 6), that is further away from the center of the deformation zone, reports an inflation rate of 15 cm/yr from 2014 to 2016 [Novoa et al., 2019].

Note again that processing the MSBAS inversion without dismissing

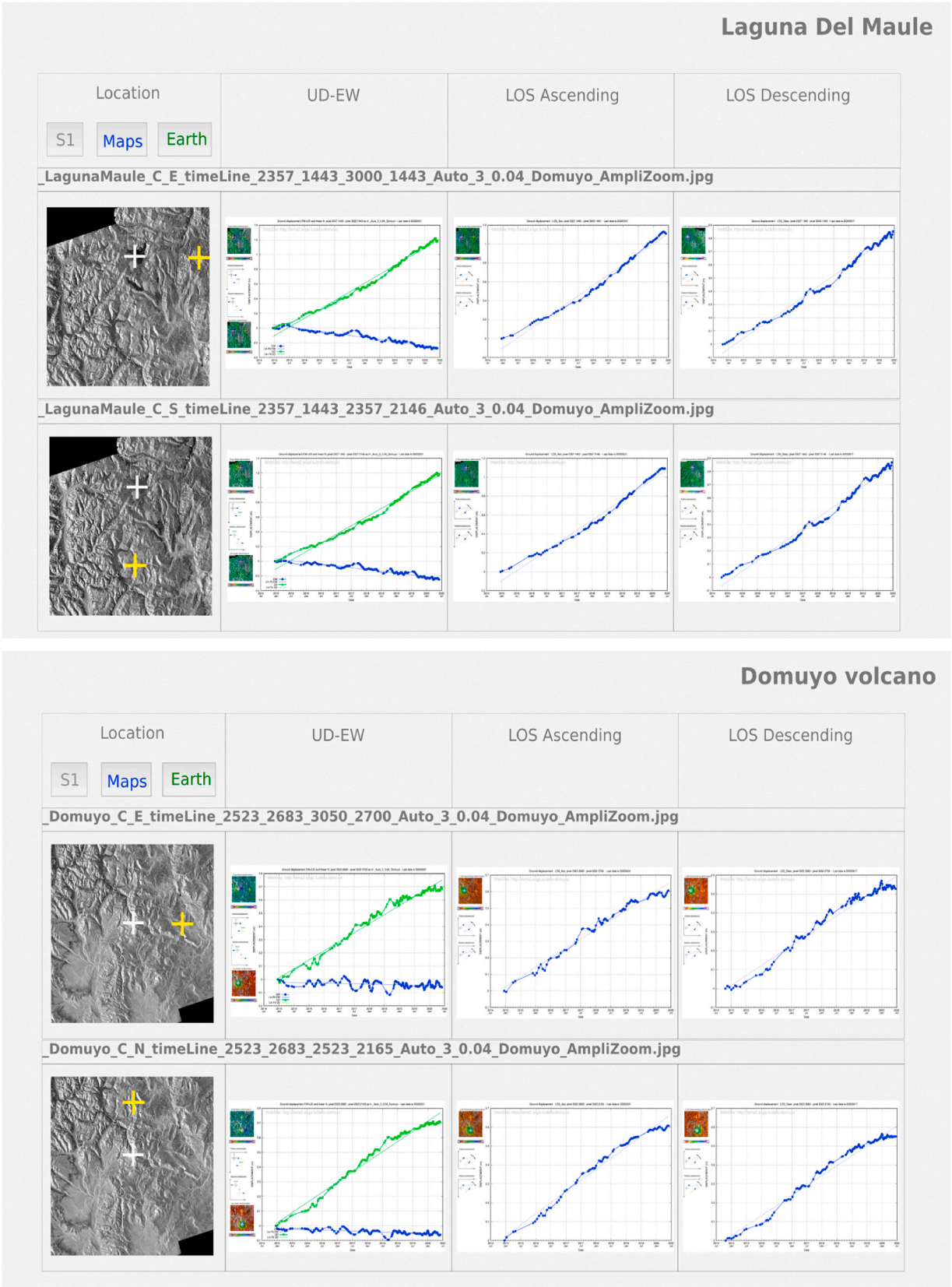

Fig. 3. Web page sample showing some automatically generated double difference time series of ground deformation spanning 2015–2020 for pairs of points at Laguna del Maule (above) and Domuyo volcano (below). For each pair of points, UD-EW graph shows Up-Down (green) and East-West (blue) displacement and Line of Sight (LOS) displacements for Ascending and Descending orbits. Clicking on these plots allows enlarged view with detailed information about direction of displacement (e.g. see Fig. 5). Note that in the present case the processing automatically rejects pairs of low coherence measured on Laguna del Maule region. It results that several images do not contribute to time series, such as those acquired during the Austral Winter. (For interpretation of the references to color in this figure legend, the reader is referred to the Web version of this article.)

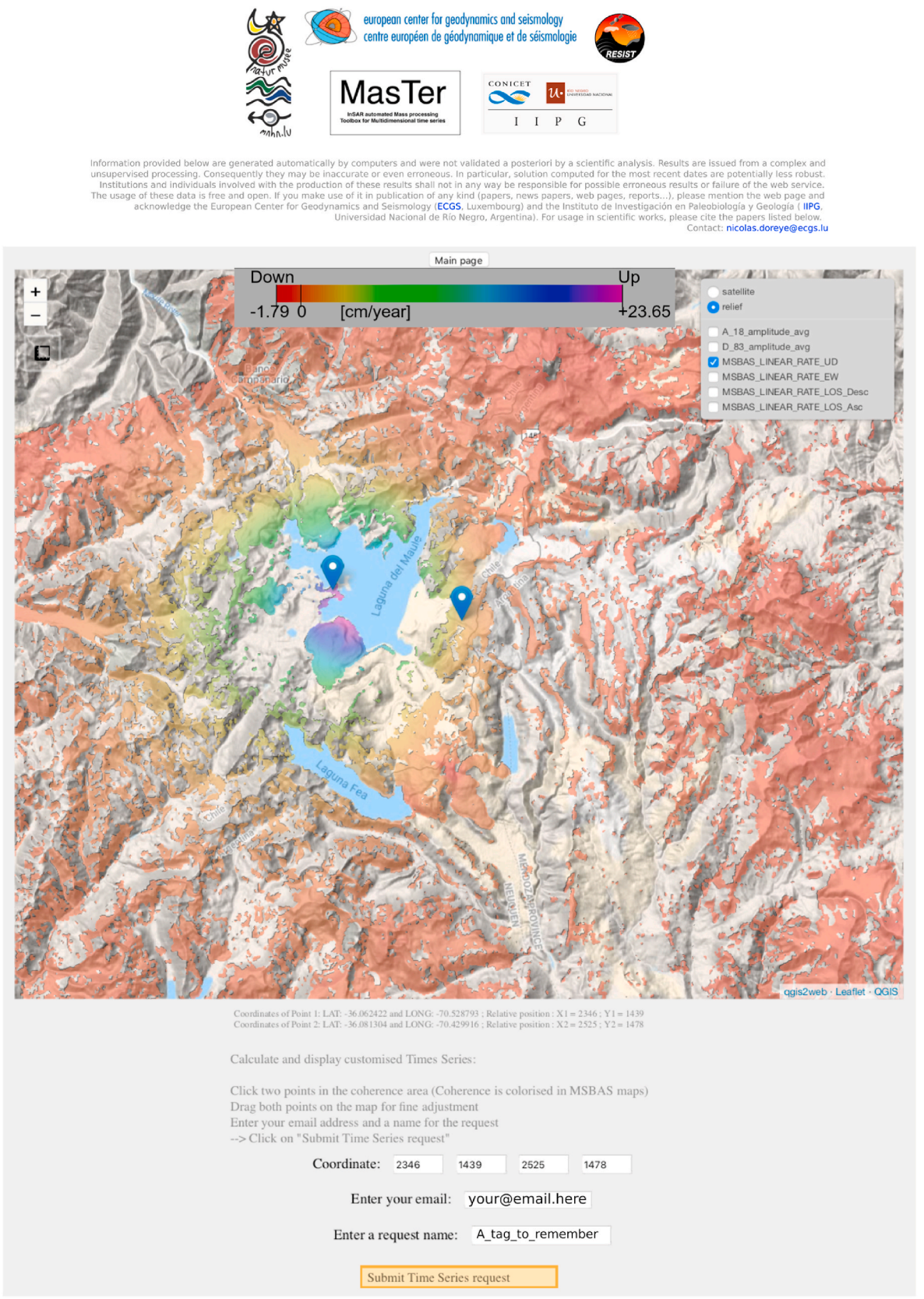

Fig. 4. Web interface allowing to request double difference time series on user-selected pair of points.

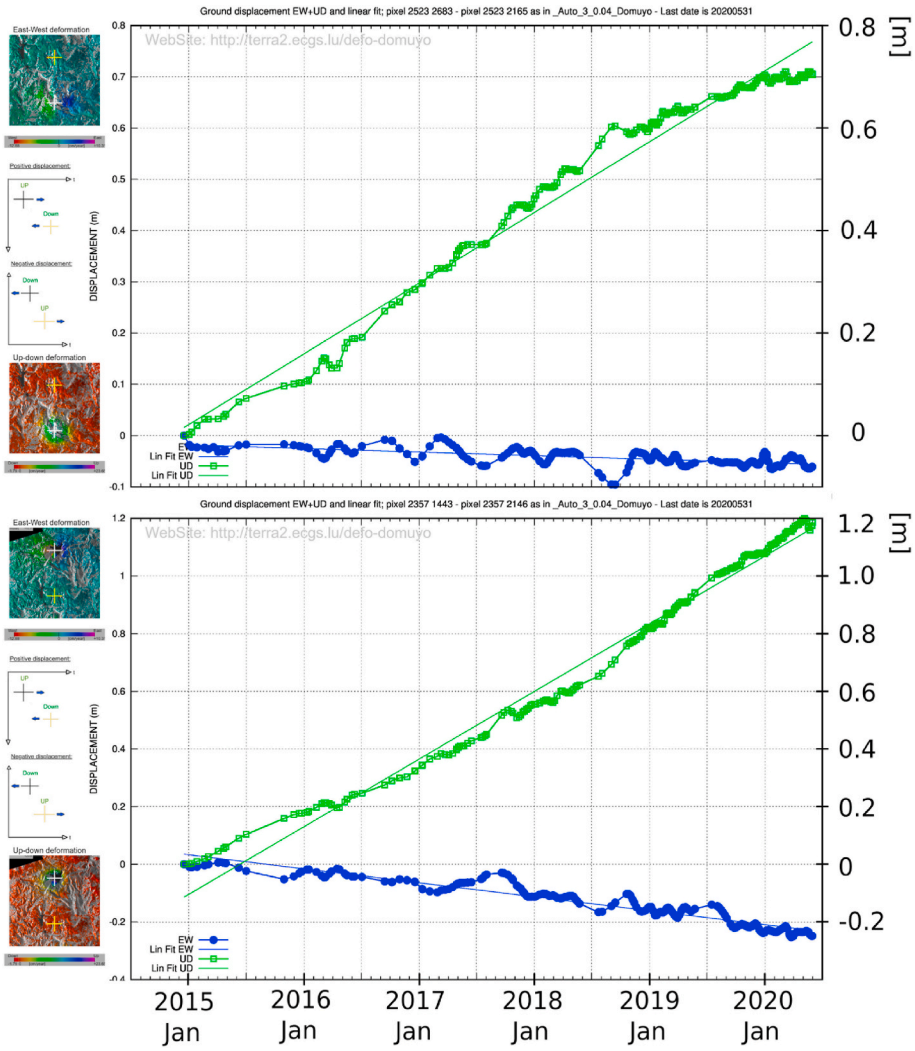

Fig. 5. Time series of vertical (green) and Est-West (blue) displacement observed at pixels located close to the center of deformation observed at Domuyo volcano (above) and Laguna del Maule (below) from October 2014 to July 2020. The displacement is computed as a double difference between the moving point and a reference point located >25 km away from the center of deformation. See location of moving points (white crosses) and references (yellow crosses) in the deformation maps to the left of figures, along with sketches helping interpreting the sense of deformation. (For interpretation of the references to color in this figure legend, the reader is referred to the Web version of this article.)

the pairs affected by seasonal decorrelation (due to snow cover during the austral winter) leads to an uplift underestimation that can be up to 45%. This underestimation is most probably due to wrongly unwrapped noisy fringes leading to underestimated differential phase for the interferogram under concern. Thanks to the high density of data offered by the Copernicus Sentinel1 mission, one can restrict a posteriori the InSAR pairs set, adding to the classical (M)SBAS criterion, a coherence threshold.

In addition to these well-known deformations at Laguna del Maule and Domuyo volcanic complexes, few additional regions affected by deformations are identified.

Fig. 6a shows a subsiding feature visible at the large coulee located to the South of Laguna del Maule. The subsidence has a crater-like circular shape, 2 km in diameter, and is located close to the southern tip of the best-fit sources used by several teams to account for the large uplift affecting the Laguna del Maule [Feigl et al., 2014; Novoa et al., 2019]. The 3 cm/yr subsidence superimposes on the uplift signal and is clearly visible e.g. on the vertical ground displacement rate profile shown in inset in Fig. 6a.

Another interesting feature is visible at a coulee located to the East of Laguna Fea (Fig. 6b). This 5 km by 1.5 km elongated coulee is affected by a steady linear movement at a pace of 2 cm/yr downward and 1 cm/yr eastward (Fig. 6b and inset). To our knowledge, this deformation was unknown or undocumented.

5. Conclusions

A fully automated DInSAR time series processing chain for displacement monitoring called MasTer (Mass processing Toolbox for Multidimensional time series) was presented. It consists in the full automation through dedicated shell scripts of Differential InSAR mass processing to feed an MSBAS processor to generate vertical and horizontal East-West displacements time series. Automation goes from data downloading to web page updating for results presentation and dissemination.

Demonstration is performed in the peculiar case of the Domuyo and Laguna del Maule volcanoes, Argentina. It allowed highlighting unreported (to our knowledge) recent changes in the well-known deformation at both volcanoes and helped identifying new deformation features at Laguna del Maule and Laguna Fea. Given its high spatial and temporal resolution and its automated processing, the tool offers efficient assistance in the monitoring of ground deformation.

The full processing chain is hosted and maintained at ECGS Luxembourg. InSAR software is maintained at LESVA. The MasTer tool is available upon request to the authors.

6. Role of funding sources

Work described in this paper is issued from several research projects and benefited from different funding sources: The RESIST project, funded by the Belgian Scientific Policy (Bel- SPo) and the Luxembourgish

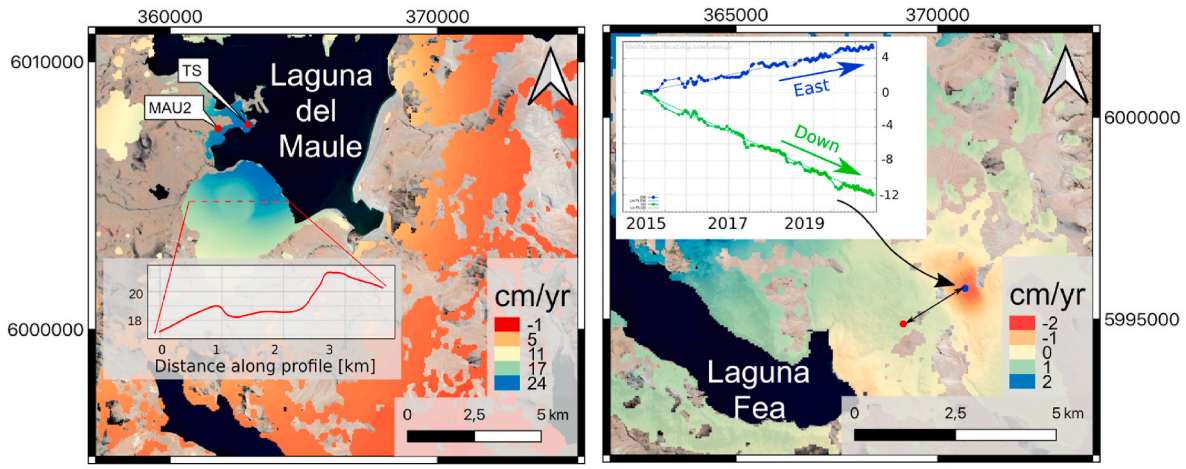

Fig. 6. a) Map of vertical linear rate at Laguna del Maule. A 2-km wide circular subsidence is clearly visible superimposed on the uplift observed at the large coulee located to the south of the lake. This roughly 3 cm/yr subsidence is illustrated with the profile of vertical ground displacement rate (inset) computed across the coulee (red dotted line). MAU2 and TS red dots locate respectively the MAU2 GNSS station [Feigl et al., 2013; Novoa et al., 2019] and the measurement of Time Series shown Fig. 5 b) Map of vertical linear rate at a coulee situated to the East of Laguna Fea. A 2 cm/yr downward and 1 cm/yr eastward movement is well tracked at the pixel located to the center of deformation. The double difference displacement in the inset shows how blue dot moves compared to red dot. That updated time series, like any other, can be consulted on the web page http://terra2.ecgs.lu/defo-domuyo. (For interpretation of the references to color in this figure legend, the reader is referred to the Web version of this article.)

National Research Fund (FNR) allowed building the required expertize while focused on Virunga Volcanic Province (Democratic Republic of Congo). The SMMIP project funded by the FNR allowed implementing and operationalizing the here-described tool. The MUZUBI project funded by BelSPo in parallel to the SMMIP project allowed adding some required specificities to the here described InSAR processor. In addition to the here above-mentioned funding sources, the National University of Rio Negro (UNRN) and CONICET, Argentina, are contributing to further software and methodology developments.

CRediT authorship contribution statement

Dominique Derauw: Conceptualization, Methodology, Software, Investigation, Writing - original draft. **d'Oreye Nicolas:** Conceptualization, Methodology, Software, Investigation, Resources, Writing - original draft. **Maxime Jaspard:** Data curation, Visualization. **Alberto Caselli:** Validation. **Sergey Samsonov:** Methodology, Software.

Declaration of competing interest

The authors declare that they have no known competing financial interests or personal relationships that could have appeared to influence the work reported in this paper.

Acknowledgments

This research took advantage of continuous improvements of both the InSAR software and the MasTer implementation during projects, namely RESIST, MUZUBI and SMMIP, principally funded by the Belgian Scientific Policy (BelSPo) and the Luxembourgish Fond National de la Recherche (FNR). MSBAS software is freely available from http://insar.ca.

Implementation of this automatized monitoring service was made possible thanks to the Copernicus Open Data Policy. Sentinel1 data were obtained from ESA at https://schihub.copernicus.eu and from ONDA DIAS at www.onda-dias.eu.

References

Andersen, N.L., Singer, B.S., Jicha, B.R., Beard, B.L., Johnson, C.M., Licciardi, J.M., 2017. Pleistocene to Holocene growth of a large upper crustal rhyoliticmagma reservoir beneath the active laguna del Maule volcanic field, central Chile. J. Petrol. 2017 (58, 1), 85–114.

Astort, Ana, Walter, Thomas R., Ruiz, Francisco, Sagripanti, Lucía, Nacif, Andrés, Acosta, Gemma, Folguera, Andrés, 2019. Detected by geophysical and geodetic dataand morphometric analysis. Remote Sens, vol. 11. Unrest at Domuyo Volcano, Argentina, p. 2175. https://doi.org/10.3390/rs11182175.

Berardino, P., Fornaro, G., Lanari, R., Sansosti, E., 2002. A new algorithm for surface deformation monitoring based on small baseline differential SAR interferograms. IEEE Trans. Geosci. Rem. Sens. 40 (11), 2375–2383. https://doi.org/10.1109/TGRS.2002.803792.

Bovenga, F., Giacovazzo, V.M., Refice, A., Veneziani, N., 2013. Multichromatic analysis of insar data. IEEE Trans. Geosci. Rem. Sens. 51 (9), 4790–4799.

Bracaccini, I.O., 1970. Rasgos tectónicos de las acumulaciones mesozoicas en las provincias de Mendoza y Neuquén. Rev. Asoc. Geol. Argent. 25, 275–282.

Brousse, R., Pesce, A.H., 1982. Cerro Domo. Un volcán Cuartario con posibilidades geotermicas. Provincia del Neuquén, in Proceedings. Congreso Latinoamericano de Geología 5th (4), 197–208.

Cardona, C., Tassara, A., Gil-Cruz, F., Lara, L., Morales, S., Kohler, P., Franco, L., 2018. Crustal seismicity associated to rpid surface uplift at Laguna del Maule Volcanic Complex, Southern Volcanic Zone of the Andes. J. Volcanol. Geoth. Res. 353, 83–94.

Chen, C.W., Zebker, H.A., 2001. Two-dimensional phase unwrapping with use of statistical models for cost functions in nonlinear optimization. J. Opt. Soc. Am. A 18, 338–351.

Chiodini, G., Liccioli, C., Vaselli, O., Calabrese, S., Tassi, F., Caliro, S., Caselli, A., Agusto, M., D'Alessandro, W., 2014. The Domuyo volcanic system: an enormous geothermal resource in Argentine Patagonia. J. Volcanol. Geoth. Res. 274, 71–77.

De Luca, C., Bonano, M., Casu, F., Manunta, M., Manzo, M., Onorato, G., Zinno, I., Lanari, R., 2018. The parallel SBAS-DInSAR processing chain for the generation of national scale sentinel-1 deformation time-series,. Procedia Computer Science 138, 326–331. https://doi.org/10.1016/j.procs.2018.10.046.

Delgado Blasco, J., Foumelis, M., Stewart, C., Hooper, A., 2019. Measuring urban subsidence in the rome metropolitan area (Italy) with sentinel-1 SNAP-StaMPS persistent scatterer interferometry, 17 Rem. Sens. 11 (2), 129. https://doi.org/10.3390/rs11020129.

Derauw, D., 1995. Phase unwrapping using coherence measurements. Synthetic aperture radar and passive microwave sensing, SPIE Proceedings. France, Paris, 21 November vol. 1995, vol. vol. 2584.

Derauw, D., 1999. Phasimétrie par Radar à Synthèse d'Ouverture; théorie et applications. PhD Thesis Université de Liège 1–141.

Derauw, D., Barbier, C., 2014. Spectral coherence applied to vessel tracking proc. IEEE Radar Conference (Radar), 2014 International 13–17. https://doi.org/10.1109/RADAR. Oct 2014, Lilles - France 7060291.

Derauw, D., Moxhet, J., Oct. 1996. Multiple images SAR interferometry. FRINGE'96 workshop, Edinburg 30 Sept - 2.

Derauw, D., Libert, L., Barbier, C., Orban, A., Kervyn, F., Samsonov, S., d'Oreye, N., 2019. The CSL InSAR Suite processor: specificities of a command line InSAR processing software specifically adapted for automated time series processing. Abstract, pp. 13–17. May 2019, ESA Living Planet Symposium 2019, Milano, Italy.

Dille, A., Dewitte, O., Handwerger, A., Derauw, D., d'Oreye, N., Moeyersons, J., Monsieurs, E., Mugaruka Bibentyo, T., Samsonov, S., Smets, B., Kervyn, M., Kervyn, F., 2020. 2020, 'Urban growth changes the pulse of a large deep-seated landslide'. EGU General Assembly 10, 5194/egusphere-egu2020-17805.

Doin, M.-P.; Lodge, F.; Guillaso, S.; Jolivet, R.; Lasserre, C.; Ducret, G.; Grandin, R.; Pathier, E.; Pinel, V.
Presentation of the small baseline NSBAS processing chain on a case example: the Etna deformation monitoring from 2003 to 2010 using Envisat data. In Proceedings of the Fringe 2011 Workshop; Frascati, Italy, 19–23 September 2011.

d'Oreye, N., Derauw, D., Libert, L., Samsonov, S., Dille, A., Nobile, A., Monsieiurs, E., Dewitte, O., Kervyn, F., May 2019. Automatization of InSAR mass processing using CSL InSAR Suite (CIS) software for Multidimensional Small Baseline Subset (MSBAS) analysis: example combining multi-satellite SAR data for landslide and volcano monitoring in South Kivu, DR Congo, Abstract. ESA Living Planet Symposium 2019. Italy, Milano, pp. 13–17.

d'Oreye, N., Derauw, D., 2020. MasTer: CSL InSAR suite automated mass processing Toolbox for multidimensional time series. User Manual version 1.4.1, Apr. 06 2020 71.

Feigl, K.L., Le Mével, H., Ali, S.T., Córdova, L., Andersen, N.L., DeMets, C., Singer, B.S., 2014. Rapid uplift in Laguna del Maule volcanic field of the Andean Southern Volcanic zone (Chile) 2007–2012. Geophys. J. Int. 196 (2), 885–901.

Ferretti, A., Prati, C., Rocca, F., 2001. Permanent scatterers in SAR interferometry. IEEE Trans. Geosci. Rem. Sens. 39 (1), 8–20. https://doi.org/10.1029/2006GL028189.

Fournier, T.J., Pritchard, M.E., Riddick, S.N., 2010. Duration, magnitude, and frequency of subaerial volcano deformation events: new results from Latin America using InSAR a global synthesis. Geochem. Geopshys. Geosyst 11 (1), 1–29, 19.

Galetto, A., García, V., Caselli, A.T., 2018. Structural controls of the Domuyo geothermal field, southern Andes (36°38′S), Argentina. J. Struct. Geol. 114, 76–94.

Galve, J., Pérez-Peña, J., Azañón, J., Closson, D., Caló, F., Reyes-Carmona, C., Jabaloy, A., Ruano, P., Mateos, R., Notti, D., et al., 2017. Evaluation of the SBAS InSAR service of the European space agency's geohazard exploitation platform (GEP), 1291 Rem. Sens. 9. https://doi.org/10.3390/rs9121291.

Goldstein, R.M., Zebker, H.A., Werner, C.L., 1988. Satellite radar interferometry: two-dimensional phase unwrapping. Radio Sci. 23, 713–720. https://doi.org/10.1029/RS023i004p00713.

Hildreth, W., Godoy, E., Fierstein, J., Singer, B., 2010. Laguna del Maule Field. Eruptive history of a quaternary basalt-to-rhyolite distributed volcanic field on the Andean range crest in central Chile, 2010. Subdirección Nacional de Geología. Sernageomin Boletin No 63, 145.

Hormes, A., Adams, M., Amabile, A.S., Blauensteiner, F., 2020. Innovative methods to monitor rock and mountain slope deformation. Geomatics and Tunnelling 13 (1), 88–102. https://doi.org/10.1002/geot.201900074.

Lazecky, M., Spaans, K., González, P.J., Maghsoudi, Y., Morishita, Y., Albino, F., Elliott, J., Greenall, N., Hatton, E., Hooper, A., Juncu, D., McDougall, A., Walters, R. J., Watson, C.S., Weiss, J.R., Wright, T.J., 2020. LiCSAR: an automatic InSAR tool for measuring and monitoring tectonic and volcanic activity. Preprints, 2020050520.

Le Mével, H., Feigl, K.L., Cordova, L., DeMets, C., Lundgren, P., 2015. Evolution of unrest at Laguna del Maule volcanic field (Chile) from InSAR and GPS measurements, 2003 to 2014. Geophys. Res. Lett. 42, 6590–6598.

Le Mével, H., Gregg, P.M., Feigl, K.L., 2016. Magma injection into long-lived reservoir to explain geodetically measured uplift: application to the 2004–2014 episode at Laguna del Maule volcanic field, Chile. J. Geophys. Res. 121, 6092–6108.

Libert, L., Derauw, D., d'Oreye, N., Barbier, C., Orban, A., 2017. Split-band interferometry- assisted phase unwrapping for the phase Ambiguities correction, 879 Rem. Sens. 9. https://doi.org/10.3390/rs9090879.

Llambías, E.J., Palacios, M., Danderfer, J.C., Brogioni, N., 1978. Petrología de las rocas ígneas cenozoicas del Volcán Domuyo y áreas adyacentes, Provincia del Neuquén, in Proceedings, Congreso Geológico Argentino, 7th. Neuquén 2, 553–584.

Lundgren, P., Girona, T., Bato, M.G., Realmuto, V.J., Samsonov, S., Cardona, C., Franco, L., Gurrola, E., Aivazis, M., 2020. The Dynamics of Large Silicic Systems from Satellite Remote Sensing Observations: the Intriguing Case of Domuyo Volcano. Scientific Reports, Argentina, pp. 1–15. https://doi.org/10.1038/s41598-020-67982-8.

Massonnet, D., Rossi, M., Carmona, C., Adragna, F., Peltzer, G., Feigl, K., Rabaute, T., 1993. The displacement field of the Landers earthquake mapped by radar interferometry. Nature 364 (6433), 138–142.

Massonnet, D., Feigl, K.L., 1998. Radar interferometry and its application to changes in the Earth's surface. Rev. Geophys. 36 (4), 441–500.

Miranda, F.J., Folguera, A., Leal, P., Naranjo, J., Pesce, A., 2006. Upper Pliocene to lower Pleistocene volcanic complexes and upper neogene deformation in the South-central Andes (36°30' – 38°S). In: Kay, S.M., Ramos, V.A. (Eds.), Evolution of an Andean margin: A Tectonic and Magmatic View from the Andes to the Neuquén Basin (35°-39°S Lat). Geol. Soc. Am. Spec. Pap., vol. 407, pp. 287–298.

Morales-Simfors, N., Bundschuh, J., Herath, I., Inguaggiatto, C., Caselli, A.T., Tapia, J., Apaza Choguhuayta, F.E., Armienta, M.A., Ormachea, M., Joseph, E., López, D.L., 2020. Arsenic in Latin America and the Caribbean: a critical overview on the geochemistry and environmental impacts of arsenic originating from geothermal features and volcanic emissions. Sci. Total Environ. https://doi.org/10.1016/j.scitotenv.2019.135564 (in press).

Nobile, A., Dille, A., Monsieurs, E., Basimike, J., Mugaruka, T.B., d'Oreye, N., Kervyn, F., Dewitte, O., 2018. Multi-temporal DInSAR to characterise landslide ground deformations in a tropical urban environment: focus on Bukavu (DR Congo). Remote sensing, 10(4), Special issue "Radar Interferometry for Geohazards" https://doi.org/10.3390/rs10040626.

Viscoelastic relaxation Novoa, C., Remy, D., Gerbault, M., Baez, J.C., Tassara, A., Cordova, L., Cardona, C., Granger, M., Bonvalot, S., Delgado, F., 2019. A mechanism to explain the decennial large surface displacements at the Laguna del Maule silicic volcanic complex. Earth and Planetary Sc. Let., 521 46–59. https://doi.org/10.1016/j.epsl.2019.06.005.

Ramos, V.A., 1977. Estructura de la Provincia de Neuquén. In Geología y recursos naturales de la Provincia del Neuquén. In: Rolleri, E.O. (Ed.), Congreso Geológico Argentino, vol. 7, pp. 9–24.

Raspini, F., Bianchini, S., Ciampalini, A., Soldato, M., Solari, L., Novali, F., Conte, S., Rucci, A., Ferretti, A., Casagli, N., 2018. Continuous, semi-automatic monitoring of ground deformation using Sentinel-1 satellites. Sci. Rep. 1–11. https://doi.org/10.1038/s41598-018-25369-w.

Samsonov, S., d'Oreye, N., 2012. Multidimensional time series analysis of ground deformation from multiple InSAR data sets applied to Virunga Volcanic Province. Geophysical Journal International, vol. 191. Iss 3, 1095–1108.

Samsonov, S., d'Oreye, N., 2017. Multidimensional small baseline Subset (MSBAS) for two-dimensional deformation analysis: case study Mexico city. Can. J. Rem. Sens. 43 (4), 318–329. https://doi.org/10.1080/07038992.2017.1344926.

Samsonov, S., d'Oreye, N., Smets, B., 2013. Ground deformation associated with post-mining activity at the French-German border revealed by novel InSAR time series method International Journal of Applied Earth Observation and Geoinformation. Int. J. Appl. Earth Obs. Geoinf. 23, 142–154. https://doi.org/10.1016/j.jag.2012.12.008.

Samsonov, S., Feng, W., Peltier, A., Geirsson, H., d'Oreye, N., Tiampo, K.F., 2017. Multidimensional Small Baseline Subset (MSBAS) for volcano monitoring in two dimensions: opportunities and challenges. Case study Piton de la Fournaise volcano. J. Volcanol. Geoth. Res. 344, 121–138. https://doi.org/10.1016/j.jvolgeores.2017.04.017.

Samsonov, S., Dille, A., Dewitte, O., Kervyn, F., d'Oreye, N., 2020. Satellite interferometry for mapping surface deformation time series in one, two and three dimensions: a new method illustrated on a slow-moving landslide. Eng. Geol. 266, 105471. https://doi.org/10.1016/j.enggeo.2019.105471.

Singer, B., Andersen, N., Le Mevel, H., Feigl, K., DeMets, C., Tikoff, B., Thurber, C., Jicha, B., Cardona, C., Cordova, L., Gil, F., Unsworth, M., Williams-Jones, G., Miller, C., Fierstein, J., Hildreth, W., Vazquez, J., 2014. Dynamics of a large, restless, rhyolitic magma system at Laguna del Maule, southern Andes, Chile. GSA Today (Geol. Soc. Am.) 24, 4–10.

Tassara, A., Yáñez, G., 2003. Relación entre el espesor elástico de la litosfera y la segmentación tectónica del margen andino (15°-47°S). Rev. Geol. Chile 30 (2), 159–186.

Tassi, F., Liccioli, C., Agusto, M., Chiodini, G., Vaselli, O., Calabrese, S., Pecoraino, G., Tempesti, L., Caponi, C., Fiebig, J., Caliro, S., Caselli, A., 2016. The hydrothermal system of the Domuyo volcanic complex (Argentina): a conceptual model based on new geochemical and isotopic evidences. J. Volcanol. Geoth. Res. 328, 198–209.

Valade, S., Ley, A., Massimetti, F., D'Hondt, O., Laiolo, M., Coppoloa, M., Loibl, D., Hellwich, O., Walter, T.R., 2019. Towards global volcano monitoring using multisensor sentinel missions and artificial intelligence: the MOUNTS monitoring system. Rem. Sens. 11, 1528,. https://doi.org/10.3390/rs11131528.

Yunjun, Z., Fattahi, H., Amelung, F., 2019. Small baseline InSAR time series analysis: unwrapping error correction and noise reduction. Comput. Geosci. 133, 104331. https://doi.org/10.1016/j.cageo.2019.104331.

Zebker, H., Villasenor, A., 1992. Decorrelation in inteferometric radar echoes. IEEE Trans. Geosci. Rem. Sens. 30, 950–959. https://doi.org/10.1109/36.175330.

Zhan, Y., Gregg, P.M., Le Mével, H., 2019. Integrating reservoir dynamics, crustal stress, and geophysical observations of the Laguna del Maule magmatic system by FEM models and data assimilation. J. Geophys. Res.: Solid Earth 124, 13,547–13,562. https://doi.org/10.1029/2019JB018681.